

# Phase transition in relaxation paths in allosteric molecules: enzymatic kinetically constrained model

Tetsuhiro S. Hatakeyama\* and Kunihiko Kaneko

*Department of Basic Science, University of Tokyo,  
3-8-1 Komaba, Meguro-ku, Tokyo 153-8902, Japan*

(Dated: July 23, 2022)

A hierarchy of timescales is ubiquitous in biological systems, where enzymatic reactions play an important role because they can hasten the relaxation to equilibrium. We introduced a statistical physics model of interacting spins that also incorporates enzymatic reactions to extend the classic model for allosteric regulation. Through Monte Carlo simulations and theoretical analysis, we found that the relaxation dynamics are much slower than the elementary reactions and are logarithmic in time with several plateaus, as is commonly observed for glasses. This is because of the kinetic constraints from the cooperativity via the competition for enzymes, which tend to bind to molecules with limited structure. This inhibits the progress of the modification reaction. Our model showed symmetry breaking in the relaxation trajectories that led to inherently kinetic phase transitions without any correspondence to the equilibrium state. In this paper, we discuss the relevance of these results for diverse responses in biology.

## I. INTRODUCTION

Biological systems are known to have a hierarchy of timescales [1]. Ordinarily, the timescale of biochemical reactions is of the subsecond order, that of organisms' behaviors is of the order of seconds to hours, and that of lifespans is of the order of years to a century. How organisms fill the gaps between such timescales is one of the most important problems in biology and physics; mechanisms that fill the gap between the timescales of biochemical reactions and organisms' behaviors have yet to be unveiled.

A biochemical process often consists of an enzymatic reaction with a complex protein, which has multiple modification sites [2–4]. The multisite modification of such molecules has recently been reported to be essential for regulating biological timescales [5–9]. Prominent examples are epigenetic regulations by histone and DNA modification; silencing gene expression by epigenetic modification takes several tens of hours, and the erasure of such memory takes a much longer time [5]. Moreover, the timescale of silencing and erasure is broadly distributed among clonal cells.

The regulation of biological timescales by multisite modification has also been observed in signaling pathways. In the Erk/Elk-1 signaling pathway, the timescales of the phosphorylation reactions of multiple phosphorylation sites are broadly distributed [6]. Mutants in which some phosphorylation sites are replaced by an amino acid mimicking the unphosphorylated state have been used to demonstrate that the phosphorylation speed of each site in multiple modification sites depends on both the site itself and the competition for Erk, which works for an enzyme.

In these examples, the modification speed of proteins with the multisite modification cannot be estimated from

the turnover rate of an enzyme or from the affinity between the substrate and the enzyme, unlike in ordinary Michaelis–Menten kinetics. Extensive theoretical studies have shown that multisite modification and the competition for an enzyme can change the kinetics as well as the steady-state modification level [7, 9, 10]. Notably, sequential multisite modification has been reported to generate a variety of timescales, some of which are much slower than the enzymatic turnover rate [10].

Such regulation of the modification kinetics, including the slow dynamics, is considered to result from intermolecular cooperativity. A dynamical-system model with chemical kinetics has previously been proposed for the average relaxation process. To reveal the intermolecular cooperativity and the fluctuations in the slow relaxation process, a model and analysis that go beyond dynamical systems are required.

Concepts from statistical physics may be useful for investigating the slow stochastic biochemical dynamics and fluctuation. Such slow dynamics have been extensively and intensively studied with regard to the physics of glasses [11]. There are two theoretical phenomenological approaches for such glassy behavior. One is the thermodynamic approach, which has been studied for the spin-glass model [12]. The energy landscape is rugged, and the state is trapped in many local energy minima; thus, relaxation to the global minimum is slowed down. The other is a kinetic constraint, in which no multiple thermodynamic metastable states exist in the energy landscape but relaxation to the equilibrium is kinetically suppressed [13]. The spin-glass model has sometimes been adopted for neural [14] and gene-regulation [15] networks. On the other hand, a promising alternative mechanism exists for kinetically slowed-down processes without resorting to the existence of multiple metastable states, namely, controlling the enzyme abundance. Because the reaction rate is controlled enzymatically, the lack of an enzyme may suppress the corresponding reactions. Despite the possible relevance of the kinetic constraint concept to

\* hatakeyama@complex.c.u-tokyo.ac.jp

biochemical processes, it has not been fully explored in biology.

In this study, to uncover a relationship between the slow dynamics in biology and the kinetic constraint, we adopted the Monod–Wyman–Changeux (MWC) model for multiple modifications of the protein state (Fig. 1). This is the classic established model for concerted allosteric regulation. The original MWC model was introduced in 1965 to explain the allosteric effect of hemoglobin against changes in the  $O_2$  concentration [16]. The model includes both the binding and unbinding of ligands and a large change in shape between the relaxed (R) and tense (T) states. When no ligands are bound, the molecule tends to be in the T state, which has a low affinity to the ligands. As ligand binding progresses, the molecule tends to be in the R state, which has a higher affinity to the ligands. Thus, ligand binding is accelerated as the ligand concentration increases, which results in the allosteric effect. We call this nonlinear change in binding the (1) *energetic effect*, which has been considered in statistical-physics models [17].

Because a modification reaction (e.g., phosphorylation, methylation, and acetylation) is generally catalyzed by an enzyme, we extended the original MWC model to incorporate kinetic facilitation by the enzyme. When the modification progresses and a molecule transitions to the R state, binding with the enzyme is accelerated, and the reaction proceeds faster. We call this the (2) *enzymatic (kinetic) effect*; this effect has not been considered in previous studies.

We used statistical physics to analyze the model by mapping the state of the MWC molecule according to the “spin.” Each molecule has a single spin representing the structural change and multiple spins representing the modification of each site. The energy of each molecule depends on the conformation of spins, and a spin flip requires the enzyme, so that both the energetic and enzymatic effects are included. Although both effects accelerate reactions, the model counterintuitively showed a slow relaxation to the equilibrium state. A typical time course for relaxation showed multiple plateaus, where the modification progress was transiently frozen far from equilibrium. The relaxation was logarithmic in time rather than exponential. Furthermore, the relaxation time did not follow the standard Arrhenius form, an exponential of the inverse temperature. The origin of such slow relaxation is explained as the decrease in the kinetic constants of reactions, which is similar to the kinetically constrained model (KCM) for glass [13]. However, in contrast to the KCMs studied thus far, the present enzymatic kinetically constrained model (eKCM) showed a phase transition of the trajectories to equilibrium rather than in the equilibrium thermodynamic quantities. We discuss the biological relevance of these results in this paper.

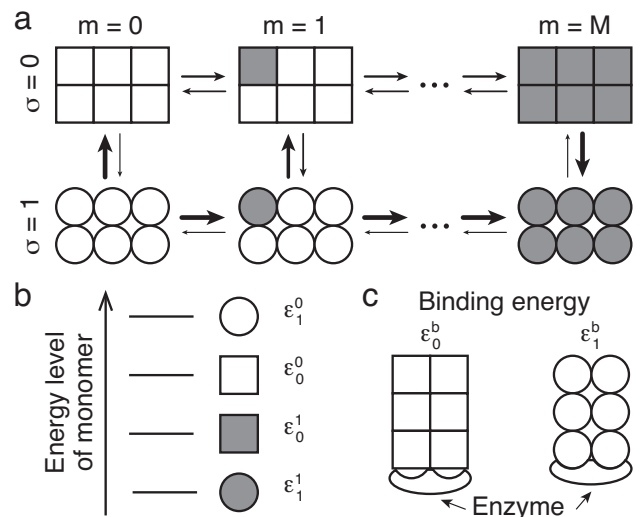


FIG. 1. Schematics of the enzymatic MWC model. (a) All states that a single MWC molecule can take.  $\sigma$  represents the T or R state and  $m$ , the number of modifications. (b) Energy level of each monomer. The total energy of each MWC molecule is given as the sum of the energies of all  $M$  (6) monomers. (c) Binding energies between the enzyme and the MWC molecules with different states. The binding energy is assumed to depend on a molecular structure represented by the state spin  $\sigma$ .

## II. MODEL

The original MWC model has two properties: modification and structural change.

(1) Modification (or ligand attachment) at several sites. Each molecule has several sites ( $M$ ) that represent multiple modification states in a single protein. (2) Structural change. When modification progresses, a protein changes its structure. If this structural change produces an allosteric effect, the protein shows a large deformation, and modification becomes more feasible. In the original MWC model, these two structures are called the T and R states [16].

As noted earlier, we represent each modification and each structural state as two types of spins; that is, each molecule has  $M$  modification spins and a single state spin taking a down or up state. Thus, each molecule has  $2^{M+1}$  states. Here, we set  $M$  as 6 unless otherwise noted. The modification spin  $s_i$  flips from 0 to 1 when each site is modified, where  $i$  is  $0 \leq i \leq M$ , and the total number of up spins is denoted as  $m$ . The structural spin  $\sigma$  flips from down to up with a structural change from the T ( $\sigma = 0$ ) state to R ( $\sigma = 1$ ) state. The internal energy of a single molecule is defined as the summation of all modification spins. Thus, the microscopic Hamiltonian of the single molecule is given as

$$\mathcal{H}(\sigma, \{s_i\}) = [m\epsilon_\sigma^1(h) + (M - m)\epsilon_\sigma^0], \quad (1)$$

where  $\epsilon_\sigma^1(h)$  and  $\epsilon_\sigma^0$  are the energies of the up and down

spins, respectively, of the  $\sigma$  state protein.  $\epsilon_\sigma^1(h)$  is a function of  $h$ , which is the ‘‘chemical field’’ derived from the concentration of the coenzyme required for the transfer of functional groups, and it is set as constant without losing generality.  $\{s_i\}$  is a set of modification spins. The number of molecules in the present system is fixed at  $N$ . We set  $N$  as 100 unless otherwise noted. Therefore, the partition function is given as

$$Z = \left[ \sum_{\sigma=0,1} \sum_i \binom{M}{i} \exp\{-\beta((M-i)\epsilon_0^\sigma + i\epsilon_1^\sigma)\} \right]^N. \quad (2)$$

Corresponding to the magnetization in the ordinary spin models, we introduce two quantitative measures: the fraction of unmodified monomers  $\mathcal{U}$  and the T-state molecule ratio  $\mathcal{T}$ . These are defined as  $1 - \sum_N m / (NM)$  and  $N_0/N = 1 - N_1/N$ , respectively, where  $N_0$  and  $N_1$  are the numbers of T-state  $\sigma = 0$  and R-state  $\sigma = 1$  molecules, respectively. Such quantities in the equilibrium state are easily derived from the partition function because there is no interaction term among the molecules in the Hamiltonian, whereas we need to specify the kinetics to study the relaxation process.

When investigating the kinetics, the allosteric effects cannot be neglected. When modification progresses, a molecule tends to flip its state, and the modification reaction is accelerated both energetically and enzymatically. Although the enzyme works as a catalyst for modification and does not change the detailed balance condition, competition for the enzyme among molecules introduces a kinetic effect rather than an energetic effect. By assuming that the timescale of enzyme binding is much faster than that of modification and state change, the binding reaction can be eliminated adiabatically. Therefore, the kinetics of the modification-spin flip are governed by the product of the binding probability ( $P_\sigma^b$ ) and the probability to traverse across the energy barrier for activation, whereas the kinetics of the state-spin flip are governed only by the latter. The energetic effect is represented by the microscopic energy of each state, whereas the enzymatic effect is represented by the changes in  $P_0^b$  and  $P_1^b$  following the state-spin flip. The two types of allosteric effects are formulated as follows.

#### (1) Energetic effect

If a molecule is modified at many modification sites, such a protein tends to change from the R state to the T state. The modification sites of R-state proteins are easier to modify than those of T-state proteins. Therefore, the energy of each modification spin has to satisfy the following inequality:

$$\epsilon_1^0 > \epsilon_0^0 > \epsilon_0^1 > \epsilon_1^1, \quad (3)$$

where  $\epsilon_1^0$ ,  $\epsilon_0^0$ ,  $\epsilon_0^1$ , and  $\epsilon_1^1$  are set to 4, 3, 2, 1, respectively.

By considering the detailed balance condition, the

transition probability of each protein state is given as

$$\frac{p(\sigma, \{1, \dots, s_M\} | \sigma, \{0, \dots, s_M\})}{p(\sigma, \{0, \dots, s_M\} | \sigma, \{1, \dots, s_M\})} = \exp(-\beta\{\epsilon_\sigma^1 - \epsilon_\sigma^0\}), \quad (4)$$

$$\frac{p(1, \{s_i\} | 0, \{s_i\})}{p(0, \{s_i\} | 1, \{s_i\})} = \exp[-\beta\{m(\epsilon_1^1 - \epsilon_0^1) + (M-m)(\epsilon_1^0 - \epsilon_0^0)\}], \quad (5)$$

where  $p(\sigma, \{1, \dots, s_M\} | \sigma, \{0, \dots, s_M\})$  and  $p(\sigma, \{0, \dots, s_M\} | \sigma, \{1, \dots, s_M\})$  are the transition probabilities for the modification and non-modification of the 1st modification spin of a  $\sigma$ -state molecule, respectively. The same transition probabilities are adopted for the other modification spins.  $p(1, \{s_i\} | 0, \{s_i\})$  and  $p(0, \{s_i\} | 1, \{s_i\})$  are the transition probabilities for the flipping of a molecule with modification state  $\{s_i\}$  from  $\sigma = 0$  to  $\sigma = 1$  and  $\sigma = 1$  to  $\sigma = 0$ , respectively.

Owing to the allosteric effect, the state tends to change to up as modification progresses; therefore, the modification spins tend to be up. When  $m$  is small, the state spin tends to be  $\sigma = 0$  because  $\epsilon_1^0 > \epsilon_0^0$ , whereas the state spin tends to be  $\sigma = 1$  because  $\epsilon_0^1 > \epsilon_1^1$  for large  $m$ . The transition probabilities from  $\sigma = 0$  to 1 and  $\sigma = 1$  to 0 are identical for  $m = M/2$ . Here, we assume that the state-flip reaction can always occur within the characteristic time of the state flip when the microscopic energy decreases. Therefore, we set the maximum value of the flip probability of the state spin as unity under the detailed balance conditions given in Eq. (5).

For the modification-spin flip, the activation energy is set to be equal to  $\epsilon_1^0$  for all modification reactions for simplicity. The modification reaction of the R-state molecule has no energy barrier and can always occur with the characteristic timescale of the modification-spin flip, whereas that of the T-state molecule has an energy barrier.

#### (2) Enzymatic (kinetic) effect

The state change between R and T increases the affinity with the enzyme; that is, it increases the probability of binding with the enzyme. As modification progresses, the fraction of R-state molecules increases, which tends to bind the enzyme more and is modified faster than the T state. We represent such an enzymatic allosteric effect by using equilibrium statistical physics. We assume that only a single enzyme can bind to the molecule. The T- and R-state molecules have different binding energies with the enzyme of  $\epsilon_0^b$  and  $\epsilon_1^b$ , respectively, where  $\epsilon_0^b$  is lower than  $\epsilon_1^b$  for the positive allosteric effect. We set  $\epsilon_0^b$  and  $\epsilon_1^b$  as 0 and 10, respectively. Thus, the transition probability for the modification reaction under the detailed balance condition (Eq. (4)) (see the Supplemental Material for the derivation):

$$\begin{aligned} p(\sigma, \{1, \dots, s_M\} | \sigma, \{0, \dots, s_M\}) &= P_\sigma^b \exp(-\beta\{\epsilon_1^0 - \epsilon_\sigma^0\}) \text{ (6)} \\ p(\sigma, \{0, \dots, s_M\} | \sigma, \{1, \dots, s_M\}) &= P_\sigma^b \exp(-\beta\{\epsilon_1^0 - \epsilon_\sigma^1\}) \text{ (7)} \\ P_\sigma^b &= \frac{\langle n_\sigma \rangle}{N_\sigma} = \frac{\exp(\beta\mu)}{\exp(-\beta\epsilon_\sigma^b) + \exp(\beta\mu)} \text{ (8)} \end{aligned}$$

where  $n_\sigma$  is the average number of enzymes that bind to

the  $\sigma$ -state molecule. Fig. S1 shows the binding probabilities calculated thus far.

We set the timescales of the modification flip and state flip as  $\tau_m$  and  $\tau_s$ , respectively, where  $\tau_m$  is longer than  $\tau_s$  ( $\tau_s = 1.0$ ,  $\tau_m = 10.0$ ). We set the initial condition such that all molecules are in the  $\sigma = 0$  and  $m = 0$  states, and we investigated the relaxation dynamics to the equilibrium state using the Monte Carlo method.

### III. RESULTS

#### eKCM shows a slow relaxation to equilibrium and multiple plateaus

First, we calculated the relaxation dynamics of  $\mathcal{U}$  and  $\mathcal{T}$ . Although  $\langle \mathcal{U} \rangle_{\text{ens}}$  and  $\langle \mathcal{T} \rangle_{\text{ens}}$ , where  $\langle \rangle_{\text{ens}}$  is the ensemble average, finally relaxed to the equilibrium values  $\mathcal{U}_{\text{eq}}$  and  $\mathcal{T}_{\text{eq}}$ , respectively, their time courses varied depending on the temperature  $1/\beta$  and  $\langle n \rangle$ , which is the number of enzymes binding to a substrate for a fixed number of molecules  $N$  (Fig. 2). When the temperature was high,  $\langle \mathcal{U} \rangle_{\text{ens}}$  decreased exponentially with time with no plateau. As the temperature decreased, the relaxation slowed down and decreased logarithmically with time. Two plateaus appeared as the temperature decreased further (see Fig. 2(a)). The two plateaus were clearly discernible when  $\langle n \rangle$  was reduced below  $\langle n \rangle / N = 0.95$ .

The value of  $\langle \mathcal{U} \rangle_{\text{ens}}$  at the plateaus increased with decreasing  $\langle n \rangle$  (see Figs. 2(b) and (c)). The relaxation of  $\langle \mathcal{T} \rangle_{\text{ens}}$  also showed a similar dependence on  $\langle n \rangle$  and the temperature, as shown in Fig. S2. Such slow dynamics with plateaus have often been observed in glasses [11].

#### Anomalous parameter dependence of the relaxation time

Glasses are known to exhibit a nonstandard temperature dependence on the relaxation time that is distinct from the normal  $\exp(E_{\text{act}}\beta)$  form derived by the standard thermal activation process with the activation energy  $E_{\text{act}}$ . To characterize the glassy phase, we computed the dependencies of the relaxation time for equilibration on  $\langle n \rangle$  and the temperature.

When the temperature was fixed and  $\langle n \rangle$  was varied, the transition probabilities for the spin modifications changed in proportion with the number of the complex  $\langle n \rangle$  in accordance with the binding probability. Indeed, for lower  $\langle n \rangle$ , the relaxation time was proportional to the inverse of  $\langle n \rangle$ . However, it was further prolonged beyond  $\langle n \rangle^{-1}$  as  $\langle n \rangle / N$  decreased to approach 1 (Fig. 3(a)). Such an  $\langle n \rangle$  dependence cannot be explained by the simple  $\langle n \rangle$  dependence of the binding probability of the enzyme.

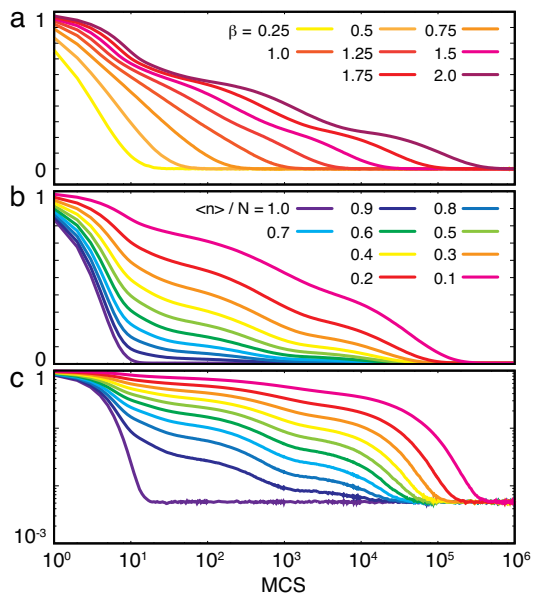


FIG. 2. Time evolution of the average modification spin in the enzymatic MWC model against the logarithmic time (Monte Carlo step). (a) Relaxation of the average number of modification spins to the equilibrium state at various temperatures. The equilibrium fraction of unmodified monomers  $\mathcal{U}_{\text{eq}}$  depends on the temperature; then, the normalized ratio  $(\langle \mathcal{U} \rangle_{\text{ens}} - \mathcal{U}_{\text{eq}}) / (1 - \mathcal{U}_{\text{eq}})$  was plotted by setting  $\langle n \rangle / N$  at 0.2. The different line colors indicate the time courses with different values of  $\beta$ . (b) Relaxation of the average modification spin to the equilibrium state for various values of  $\langle n \rangle$ . The time course of  $\langle \mathcal{U} \rangle_{\text{ens}}$  was plotted by setting  $\beta$  at 1.75. The different line colors correspond to different values of  $\langle n \rangle / N$ . ( $\mathcal{U}_{\text{eq}}$  is independent of  $\langle n \rangle$ ). Each line is an ensemble average of 1000 samples. (c) Logarithm of  $\langle \mathcal{U} \rangle_{\text{ens}}$  plotted for (b).

The relaxation time also showed an anomalous temperature dependence. Because the energy barrier for the modification of the T-state molecule was set to unity while the modification of the R-state molecule was temperature-independent, the relaxation time would normally be expected to be proportional to  $\exp(\beta)$ . Indeed, at high temperatures, the relaxation time approximately followed  $\exp(\beta)$ . However, as the temperature decreased, the rate of increase in the relaxation time against the temperature was enhanced and reached its maximum at around  $\beta = 1$ . The relaxation time showed a bending point around  $\beta \sim 1$ , and for low temperatures, it approximately obeyed  $\exp(6\beta)$  (see Fig. 3(b)). The fact that the activation energy is six times the energy barrier for each modification (see Fig. 1) suggests that the transition from the  $(m = 0, \sigma = 0)$  state to the  $(m = 0, \sigma = 1)$  state is rate-limiting.

The two salient features, namely, the plateaus and anomalous parameter sensitivity of the relaxation time, suggest that the present model has characteristics similar to those of glasses.

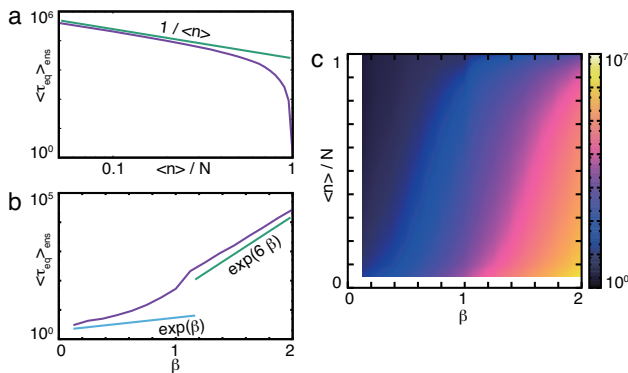


FIG. 3. Relaxation times at various temperatures and  $\langle n \rangle$  values. (a) Dependence of the relaxation time on  $\langle n \rangle / N$ . The relaxation time is defined as the ensemble average of  $\tau_{\text{eq}}$  when  $\mathcal{T}$  falls below the analytically calculated value  $\mathcal{T}_{\text{eq}}$  because  $\mathcal{T}$  approaches equilibrium from above. The green line indicates a line proportional to  $\langle n \rangle^{-1}$ .  $\beta$  was set at 1.75. (b) Dependence of the relaxation time on the temperature. The blue and green lines indicate lines proportional to  $\exp(\beta)$  and  $\exp(6\beta)$ , respectively.  $\langle n \rangle / N$  was set at 0.8. (c) Logarithmic average of the relaxation time.  $\log_{10} \langle \tau_{\text{eq}} \rangle_{\text{ens}}$  against  $\beta$  and  $\langle n \rangle / N$  is shown using the colors in the side bar.

### Phase transition of the relaxation trajectories in the eKCM

To reveal the mechanism of the anomalous parameter dependence, we analyzed the relaxation-time distribution over the samples. In the region where the relaxation time showed anomalous parameter dependence, the relaxation-time distribution changed from unimodal to multimodal (Fig. 4). The multiple peaks that emerged are named the first, second, and third peaks in ascending order of relaxation time.

When  $\langle n \rangle$  was varied at a fixed temperature, the positions of the peaks changed in proportion to  $\langle n \rangle^{-1}$  (see Fig. 4(a)). Thus, we studied the distribution of the relaxation time normalized by  $\langle n \rangle^{-1}$ . When  $\langle n \rangle / N$  was close to 1, two peaks were observed. As  $\langle n \rangle$  decreased, the first peak disappeared and was replaced by the third one. Finally, the second peak disappeared completely at  $\langle n \rangle / N = 0.4$ . This change in the distribution is similar to the first-order phase transition in equilibrium thermodynamics. The transition here, however, was with regard to the relaxation time rather than the thermodynamic quantities. It should be recalled that the same equilibrium state was reached over all samples independent of the relaxation courses. This multimodal distribution of the relaxation time was concerned with the transition of the trajectories.

As  $M$  was increased, the divergence of the relaxation-time against  $\langle n \rangle / N \rightarrow 1$  was steeper (Fig. 4(d)) and its variance increased (Fig. S3). This suggests that in the limit of  $M \rightarrow \infty$  and  $N \rightarrow \infty$ , the change in the relaxation time will be the phase transition in the

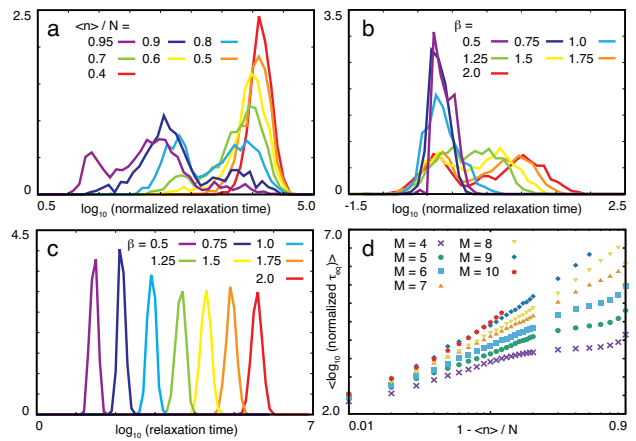


FIG. 4. Probability distributions of the relaxation time at various temperatures and  $\langle n \rangle$  values and the variance of the logarithmic relaxation time. (a) Probability distribution of the logarithmic normalized relaxation time at various  $\langle n \rangle$  values with fixed temperature at  $\beta = 1.75$ . The logarithmic relaxation time was calculated as the base-10 logarithm of  $\tau_{\text{eq}}$  and rescaled by  $\tau_{\text{eq}} \langle n \rangle^{-1}$ . Different color lines indicate the probability distributions with different  $\langle n \rangle$ s. (b) Probability distribution of the logarithmic normalized relaxation time at various temperatures with  $\langle n \rangle / N$  fixed at 0.8. The plot is rescaled by  $\tau_{\text{eq}} e^{-4\beta}$ . The lines with different colors indicate the probability distributions at different temperatures. (c) Probability distribution of the logarithmic relaxation time at various temperatures with  $\langle n \rangle / N$  fixed at 0.2. (d) Averaged normalized relaxation time for different number of modification sites  $M$  indicated by different symbols. The plot is rescaled in the similar way as in (a).

context of statistical physics. Indeed, as  $N$  increased, the divergence of the relaxation time was steeper even in the case of  $N = 6$  (see Fig. S4).

The temperature dependence of the relaxation-time distribution when  $\langle n \rangle / N$  was fixed close to 1 differed from its  $\langle n \rangle$  dependence (see Fig. 4(b)). In this case, the position of the first peak changed in proportion to  $\exp(4\beta)$ , as explained later. At high temperatures, the relaxation-time distribution was unimodal. This distribution broadened with decreasing temperature at around  $\beta = 1.0$ , where it became bimodal, and the distance between these two peaks increased with decreasing temperature. This change in the relaxation-time distribution is similar to the second-order phase transition in equilibrium.

This transition is caused by kinetic constraint from the competition for the enzyme among R- and T-state molecules. As the relaxation progresses and the number of R-state molecules reaches almost the same level as that of the enzyme, the R-state molecules monopolize the enzyme due to the positive allosteric effect (see Fig. S1). Then, further progress in the modification reactions of the T-state molecules is difficult (see Fig. 5(a)). In this situation, the transition from the T- to the R-state is rate-limiting with three possible steps,  $m = 0, 1$ , and

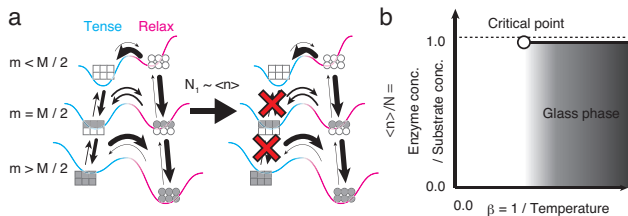


FIG. 5. (a) Schematic showing the energy landscape of the enzymatic MWC model. (Left) If the number of R-state molecules is lower than that of the enzyme, the modification reaction of T-state molecules (up and down arrows) can occur and progress until half of the modification sites are modified. Then, when more than half of the sites are modified, such molecules tend to be in the R state (lower right arrow). (Right) When the number of R-state molecules exceeds that of the enzyme through modification, the R-state molecules monopolize the enzyme, and the modification reaction of T-state molecules is kinetically inhibited (red crosses). Therefore, the structural changes from the T- to R-state in the less modified molecules (upper right arrow) are rate-limiting. (b) Phase diagram of the glass transition of paths.

2, having the energy barriers 6, 4, and 2, respectively. Thus, the temperature dependence of the transition rate follows  $\exp(6\beta)$  ( $m = 0$ ),  $\exp(4\beta)$  ( $m = 1$ ), and  $\exp(2\beta)$  ( $m = 2$ ). These rate-limiting steps correspond to the third, second, and first peaks in Fig. 4(a), respectively, and the three plateaus of relaxation (Fig. 2).

When the number of molecules is finite, the rate-limiting step depends on the distribution of the phosphorylation level of the T-state molecules at the start of the kinetically constrained condition. As long as the ( $m = 0, \sigma = 0$ ) molecule exists, the transition from ( $m = 0, \sigma = 0$ ) to ( $m = 0, \sigma = 1$ ) is rate-limiting, whereas if it is not included, its transition from ( $m = 1, \sigma = 0$ ) to ( $m = 1, \sigma = 1$ ) is rate-limiting as long as the  $m = 1$  molecule exists, and so forth. Indeed, only the samples in the peak with the longest relaxation time and having three plateaus had molecules in the  $m = 0$  state (see Fig. S5). This suggests that the fluctuation in the distribution of molecular states at the beginning of relaxation affects the entire process in the trajectory.

Based on the above considerations, the multimodal distribution of the logarithmic relaxation time is an important indicator of the transition to the glass phase. Indeed, the variance of the logarithmic relaxation time is large at the upper boundary of the glass phase (Fig. S6(a)), whereas the relaxation-time distribution does not show a transition from unimodal to multimodal when we change the temperature with a fixed small  $\langle n \rangle$  (Fig. 4(c)). This suggests that such a change is a crossover rather than a transition (see also Fig. 5(b)). In fact, there was no change in the appearance of the plateaus at low  $\langle n \rangle$  values, as shown in Fig. 2(a).

## IV. DISCUSSION

We propose a statistical physics model for allosteric biomolecules and enzymes that catalyze the modification reaction of the allosteric molecules. The present model showed a slow relaxation to equilibrium with several plateaus, in which the relaxation time depended anomalously on the temperature. This behavior is known in glass theory. In our model, the kinetic constraint is autonomously imposed by competition for the enzyme among T- and R-state molecules, resulting in the glassy relaxation. In consistency with the standard KCM, the present kinetic constraint is generated and controlled by the enzyme abundance, which works as a parameter for the phase transition; therefore, it is termed as eKCM.

The relaxation of modification of the T-state molecules is frozen by the competition for the enzyme, whereas the R-state molecules are partially equilibrated. This is similar to the dynamical heterogeneity, which is important in glass theory [18]. The number of frozen molecules depends on the history and differs for each replicate (Figs. S7 and S8). The variance in modification level approaches  $M$  through the relaxation (see Fig. S7). This reflects the MWC-type allostery, where all the  $M$  monomers flip their molecular structure cooperatively.

The eKCM exhibited the phase transition in the relaxation paths to equilibrium, depending on the temperature and the enzyme concentration. Following the phase transition of the trajectories, slow relaxation and plateaus appeared, as in the glass transition. However, most of the KCMs studied thus far do not show the phase transition of paths with change in temperature [13], and needless to say, there is no external parameter corresponding to the enzyme abundance. In the eKCM, the strength of the cooperativity in kinetics depends on the enzyme abundance and temperature. When the amount of enzyme is greater than that of the substrate, there is no competition, and glassy behavior does not appear. The competition for a limited amount of the enzyme introduces interactions among molecules, resulting in the transition to a state with heterogeneity in the relaxation paths.

The phase transition discovered in this study is considered to be a new nonequilibrium phase transition, in contrast to those concerned with the steady state, as previously reported [19–21]. In the KCMs of glasses, discussions on such phase transitions have been limited to that against the “activity” [22], which is a fictitious parameter introduced for large-deviation analysis and not a real parameter that can be controlled, as in the enzyme abundance in our model. We expect that further analysis of the eKCM will lead to deeper understanding of the nonequilibrium phase transition with glass behavior.

In recent decades, the slow relaxation process has also attracted much interest in the field of biology. In bacterial chemotaxis, chemoreceptors, which are often described by an MWC-type model [23, 24], are known to form clusters with each other. A recent experiment

demonstrated that such chemoreceptor clusters show a slow logarithmic change in their structure with time in response to the addition and removal of a ligand [25]. This slow relaxation is a result of the interactions among the chemoreceptors that modify their structures without using a specific adaptation by signaling enzymes (cheR and cheB), as in our study. Logarithmic relaxation without plateaus was observed in the experiment, as was also seen in our model around the critical temperature. To find further correspondence between theory and experiments on the chemoreceptor cluster, a two-dimensional space should be considered in the eKCM.

Another biological example that corresponds with our theory is  $\text{Ca}^{2+}$ /calmodulin-dependent protein kinase II (CaMKII), which is known to be important for maintaining long-term potentiation in a synapse [26]. The structural changes in CaMKII that accompany phosphorylation are sustained over a few minutes after a stimulus in the hippocampal synapse [27]. On the other hand, it was recently suggested that the phosphorylation of CaMKII in the dorsal raphe nucleus regulates the sleep–awake cycle, particularly the length of sleeping hours (i.e., typically 6 h) [28]. These results suggest that the phosphorylation of CaMKII can show various timescales during relaxation, ranging from minutes to hours, as shown in our study.

Other candidates for the eKCM are the proteins incorporated into the circadian clock. In particular, phosphorylation of PER2 by a kinase,  $\text{CKI}\epsilon/\delta$ , determines the period of the mammalian circadian clock [30]. Interestingly,  $\text{CKI}\epsilon/\delta$  tends to bind its own catalytic products, which is consistent with our positive allostery. Further, mice with a mutant that lowers such  $\text{CKI}\epsilon/\delta$ -binding activity showed a shorter period of circadian rhythm [31], suggesting that the timescale regulation by our mechanism may be useful there. Future experiment by using mutated clock-protein mimicking (un)modified residues,

as performed in the experiment related to Elk-1 [6], is expected.

Our study also demonstrated that microscopic fluctuation in molecular states can be amplified to a large variation in the relaxation time. Although the noise in chemical concentrations has recently attracted much attention from many physicists and biologists [29], there has been little study on the fluctuations in the relaxation paths in biology. They can be easily observed experimentally by using a biochemical reaction in a liposome or emulsion, as larger fluctuations are expected for a system with a small number of molecules.

The slow relaxation we showed is robust against fluctuations in the enzyme amount and temperature, as long as the system is not close to the critical point. The relaxation time changes continuously and its variance remains small. In contrast, near the critical point, cells with the same genetic and environmental backgrounds can have a large variance in the relaxation time and different fates. Such fluctuation in the timescale will also be useful for dynamic bet hedging; multiple timescales among the clonal population will help an organism to adapt to a fluctuating and repeating environment.

We expect that the experiments mentioned above with chemoreceptors, CaMKII, and clock proteins will demonstrate the slow relaxation of modifications as well as large variance of relaxation time, and deepen our understanding of the relationship between the regulation of biological timescales and glass theory in physics.

## ACKNOWLEDGEMENTS

We thank Atsushi Ikeda for critical reading of the manuscript and Yasushi Okada and Tom Shimizu for helpful discussions. This work was partially supported by Grants-in-Aid for Scientific Research, KAKENHI, grant number 17H05758.

- 
- [1] R. Phillips, J. Kondev, and J. Theriot, *Physical Biology of the Cell* (Garland Science, Taylor & Francis Group, New York, 2008).
  - [2] C. Walsh, *Posttranslational Modification of Proteins: Expanding Natures Inventory* (Roberts and Company Publishers, Colorado, 2006).
  - [3] P. Cohen, The role of protein phosphorylation in human health and disease, *Eur. J. Biochem.* **268**, 19 (2001).
  - [4] E. Li, Chromatin modification and epigenetic reprogramming in mammalian development, *Nat. Rev. Genet.* **3**, 9 (2002).
  - [5] L. Bintu, J. Yong, Y. E. Antebi, K. McCue, Y. Kazuki, N. Uno, M. Oshimura, and M. B. Elowitz, Dynamics of epigenetic regulation at the single-cell level, *Science* **351**, 6274 (2016).
  - [6] A. Mylona, F. X. Theillet, C. Foster, T. M. Cheng, F. Miralles, P. A. Bates, P. Selenko, and R. Treisman, Opposite effects of Elk-1 multisite phosphorylation shape its response to ERK activation, *Science* **354**, 6309 (2016).
  - [7] C. Salazar and T. Höfer, Multisite protein phosphorylation – From molecular mechanisms to kinetic models, *FEBS J.* **276**, 12 (2009).
  - [8] M. Zhou, J. K. Kim, G. W. L. Eng, D. B. Forger, and D. M. Virshup, A period2 phosphoswitch regulates and temperature compensates circadian period, *Mol. Cell* **60**, 1 (2015).
  - [9] T. S. Hatakeyama and K. Kaneko, Generic temperature compensation of biological clocks by autonomous regulation of catalyst concentration, *Proc. Natl. Acad. Sci. USA* **109**, 21 (2012).
  - [10] T. S. Hatakeyama and K. Kaneko, Kinetic memory based on the enzyme-limited competition, *PLoS Comput. Biol.* **10**, 8 (2014).
  - [11] P. G. Debenedetti and F. H. Stillinger, Supercooled liquids and the glass transition, *Nature* **410**, 6825 (2001).

- [12] M. Mézard and A. Montanari, *Information, Physics, and Computation* (Oxford University Press, New York, 2009).
- [13] F. Ritort and P. Sollich, Glassy dynamics of kinetically constrained models, *Adv. Phys.* **52**, 4 (2003).
- [14] D. J. Amit, H. Gutfreund, and H. Sompolinsky, Spin-glass models of neural networks, *Phys. Rev. A* **32**, 2 (1985).
- [15] M. Sasai and P. G. Wolynes, Stochastic gene expression as a many-body problem, *Proc. Natl. Acad. Sci. USA* **100**, 5 (2003).
- [16] J. Monod, J. Wyman, and J. -P. Changeux, On the nature of allosteric transitions: A plausible model, *J. Mol. Biol.* **12** (1965).
- [17] S. Marzen, H. G. Garcia, and R. Phillips, Statistical mechanics of Monod–Wyman–Changeux (MWC) models, *J. Mol. Biol.* **425**, 9 (2013).
- [18] L. Berthier, G. Biroli, J. -P. Bouchaud, L. Cipelletti, and W. van Saarloos (Eds.), *Dynamical Heterogeneities in Glasses, Colloids, and Granular Media* (Oxford University Press, New York, 2011).
- [19] A. L. Barabási and H. E. Stanley, *Fractal Concepts in Surface Growth* (Cambridge University Press, Cambridge, 1995).
- [20] D. E. Wolf, M. Schreckenberg, and A. Bachem (Eds.) *Traffic and Granular Flow* (World Scientific, Singapore, 1996).
- [21] H. Hinrichsen, Non-equilibrium critical phenomena and phase transitions into absorbing states, *Adv. Phys.* **49**, 7 (2000).
- [22] J. P. Garrahan, R. L. Jack, V. Lecomte, E. Pitard, K. van Duijvendijk, and F. van Wijland, Dynamical first-order phase transition in kinetically constrained models of glasses, *Phys. Rev. Lett.* **98**, 19 (2007).
- [23] S. Asakura and H. Honda, Two-state model for bacterial chemoreceptor proteins: The role of multiple methylation, *J. Mol. Biol.* **176**, 3 (1984).
- [24] G. Lan and Y. Tu, Information processing in bacteria: Memory, computation, and statistical physics: A key issues review, *Reports. Prog. Phys.* **79**, 5 (2016).
- [25] V. Frank and A. Vaknin, Prolonged stimuli alter the bacterial chemosensory clusters, *Mol. Microbiol.* **88**, 3 (2013).
- [26] J. Lisman, R. Yasuda, and S. Raghavachari, Mechanisms of CaMKII action in long-term potentiation, *Nat. Rev. Neurosci.* **13**, 3 (2012).
- [27] S. -J. R. Lee, Y. Escobedo-Lozoya, E. M. Szatmari, and R. Yasuda, Activation of CaMKII in single dendritic spines during long-term potentiation, *Nature* **458**, 7236 (2009).
- [28] S. Y. Cui et al., Phosphorylation of CaMKII in the rat dorsal raphe nucleus plays an important role in sleep-wake regulation, *J. Neurochem.* **136**, 3 (2016).
- [29] M. B. Elowitz, A. J. Levine, E. D. Siggia, and P. S. Swain, Stochastic gene expression in a single cell, *Science* **297**, 5584 (2002).
- [30] Y. Isojima et al.,  $CKI\epsilon/\delta$ -dependent phosphorylation is a temperature-insensitive, period-determining process in the mammalian circadian clock, *Proc. Natl. Acad. Sci. USA* **106**, 37 (2009).
- [31] Y. Shinohara et al., Temperature-sensitive substrate and product binding underlie temperature-compensated phosphorylation in the clock, *Mol. Cell* **67**, 5 (2017).

Supplemental materials for  
 “Phase transition in relaxation paths in allosteric  
 molecules: enzymatic kinetically constrained  
 model”

Tetsuhiro S. Hatakeyama\*and Kunihiko Kaneko

*Department of Basic Science, University of Tokyo, 3-8-1 Komaba,  
 Meguro-ku, Tokyo 153-8902, Japan*

## 1 Derivation of the binding probability of the enzyme

We assume that only a single enzyme can bind to the molecule. The T- and R-state molecules have different binding energies with the enzyme of  $\epsilon_0^b$  and  $\epsilon_1^b$ , respectively, where  $\epsilon_0^b$  is lower than  $\epsilon_1^b$  for the positive allosteric effect. Therefore, the grand partition function and the average number of binding enzymes  $\langle n \rangle$  in equilibrium are represented in a similar manner as Langmuir’s adsorption isotherm [1] and are given as

$$\Xi = \left\{ 1 + \exp(\beta(\epsilon_0^b + \mu)) \right\}^{N_0} \left\{ 1 + \exp(\beta(\epsilon_1^b + \mu)) \right\}^{N_1}, \quad (1)$$

$$\langle n \rangle = N_0 \frac{\exp(\beta\mu)}{\exp(-\beta\epsilon_0^b) + \exp(\beta\mu)} + N_1 \frac{\exp(\beta\mu)}{\exp(-\beta\epsilon_1^b) + \exp(\beta\mu)}. \quad (2)$$

For both *in vivo* and *in vitro* reactions,  $N$  and  $n$  are almost constant and are the control parameters of the system. Here, we assume that  $\langle n \rangle$  is the same as  $n$ , which is the total number of enzymes in the system, and that the chemical potential  $\mu$  is a function of  $\langle n \rangle$ ,  $N_0$ , and  $N_1 = N - N_0$ .

---

\*hatakeyama@complex.c.u-tokyo.ac.jp

This assumption is justified when  $N$  and  $n$  are sufficiently large, i.e., at the thermodynamic limit. Then,  $\exp(\beta\mu)$  is given as

$$\exp(\beta\mu) = \frac{-A + \sqrt{A^2 - 4 \langle n \rangle (\langle n \rangle - N) \exp(-\beta(\epsilon_0^b + \epsilon_1^b))}}{2(\langle n \rangle - N)}, \quad (3)$$

where  $A = (\langle n \rangle - N + N_0) \exp(-\beta\epsilon_0^b) + (\langle n \rangle - N_1) \exp(-\beta\epsilon_1^b)$ . In the limit  $\langle n \rangle \rightarrow N$ ,  $\mu$  approaches  $-\infty$ , and all molecules bind to the enzyme. The arguments so far can be summarized to give the binding probability

$$P_\sigma^b = \frac{\langle n_\sigma \rangle}{N_\sigma} = \frac{\exp(\beta\mu)}{\exp(-\beta\epsilon_\sigma^b) + \exp(\beta\mu)}, \quad (4)$$

where  $n_\sigma$  is the average number of enzymes that bind to the  $\sigma$ -state molecule.

It is noted that in the thermodynamic limit, the binding reaction is described by the Michaelis–Menten equation for the timescale separation. The Michaelis–Menten equation for multiple substrates with the conservation of the enzyme concentration is given as

$$N_E^{\text{tot}} = \frac{N_{S0}N_E^{\text{free}}}{K_0 + N_E^{\text{free}}} + \frac{N_{S1}N_E^{\text{free}}}{K_1 + N_E^{\text{free}}} + N_E^{\text{free}}, \quad (5)$$

where  $N_E^{\text{tot}}$  is the concentration of all enzymes,  $N_E^{\text{free}}$  is the concentration of free enzymes that do not bind to any substrate,  $N_{S_i}$  is the concentration of the  $i$ -th substrate, and  $K_i$  is the dissociation constant between the enzyme and the  $i$ -th substrate. A comparison of Eqs. (2) and (5) indicates that  $\exp(-\beta\epsilon_\sigma^b)$  is  $K_\sigma$ ,  $\exp(\beta\mu)$  is  $N_E^{\text{free}}$ , and  $\langle n \rangle$  is  $N_E^{\text{tot}} - N_E^{\text{free}}$ . If  $N_E^{\text{tot}}$  is smaller than  $N_{S0} + N_{S1}$  and  $K_i$  is much smaller than  $S_i$ , almost all enzymes bind to substrates; that is,  $\langle n \rangle \simeq N_E^{\text{tot}}$ . Under this condition,  $N_{S0}N_E^{\text{free}}/(K_0 + N_E^{\text{free}})$  and  $N_{S1}N_E^{\text{free}}/(K_1 + N_E^{\text{free}})$  have to be  $\mathcal{O}(N_E^{\text{tot}})$ , where  $\mathcal{O}$  is the Landau notation. Thus,  $N_E^{\text{free}}$  is estimated as  $N_E^{\text{free}}/N_E^{\text{tot}} \sim K_i/N_{S_i}$ . Thus, when the substrates have sufficiently large binding energies for the enzyme,  $N_E^{\text{free}}$  is negligible compared with  $N_E^{\text{tot}}$ , and  $\langle n \rangle$  is considered to be constant throughout the relaxation process for actual *in vivo* and *in vitro* reactions. In contrast, when  $N_E^{\text{tot}}$  is higher than  $N_{S0} + N_{S1}$ ,  $\langle n \rangle/N$  is 1 through the relaxation process for a sufficiently small binding energy.

## 2 Variance among samples

Interestingly, the variance of  $\langle \mathcal{U} \rangle_{\text{ens}}$  or  $\langle \mathcal{T} \rangle_{\text{ens}}$  with the samples increased at the initiation of the plateaus (Fig. S7). The maximum variance,

which was normalized by division by the average over the samples, increased gradually with decreasing temperature (see Fig. S7(a)). This corresponded to the gradual appearance of the plateau in the averaged relaxation dynamics (Fig. 2(a) in the main text). As  $\langle n \rangle$  decreased, the change in the variance became more drastic. When  $\langle n \rangle / N$  was 1, there was only one peak at an early step (see the purple line in Fig. S7(b)). At  $\langle n \rangle / N = 0.9$ , a second plateau appeared suddenly in the average relaxation dynamics (see Fig. 2(b) in the main text). Accordingly, a second peak in the variance appeared suddenly (see the blue line in Fig. S7(b)). The variance increased at the beginning of the plateaus because the number of modified spins varied with each sample, and the induced variance froze at the plateaus (see Fig. S8). Therefore, the variance among samples provided a good indicator of the plateaus.

To clarify the region where multiple plateaus appear, we plotted the maximum variance after the first peak by subtracting the equilibrium value of the variance (Fig. S6(b)). The diagram shows that the variance was high under low- $\langle n \rangle$  and low-temperature conditions, which indicates the existence of multiple plateaus similar to glassy dynamics. Accordingly, we call this region the “glass phase.”

## References

- [1] Phillips R, Kondev J, Theriot J (2008) *Physical Biology of the Cell* (Garland Science, Taylor & Francis Group, New York).

## 3 Supporting figures

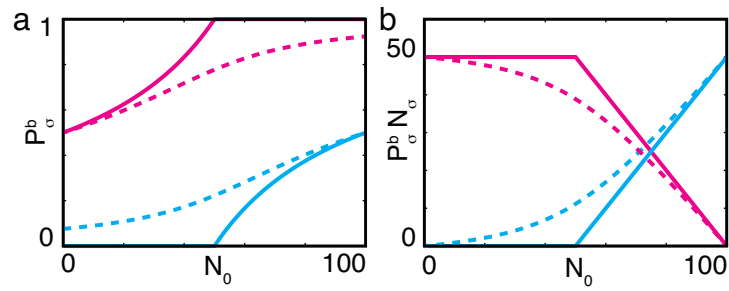


Figure S 1: Binding probability between the enzyme and the substrates. (a) Binding probability ( $P_\sigma^b$ ) and (b) the number of complexes ( $P_\sigma^b N_\sigma$ ) for different substrates at different temperatures. Cyan and magenta represent  $\sigma = 0$  and  $\sigma = 1$  substrates, respectively. Solid and dashed lines represent  $\beta = 1.75$  and  $0.25$ , respectively.  $N$  and  $\langle n \rangle / N$  were set to 100 and 0.5, respectively.

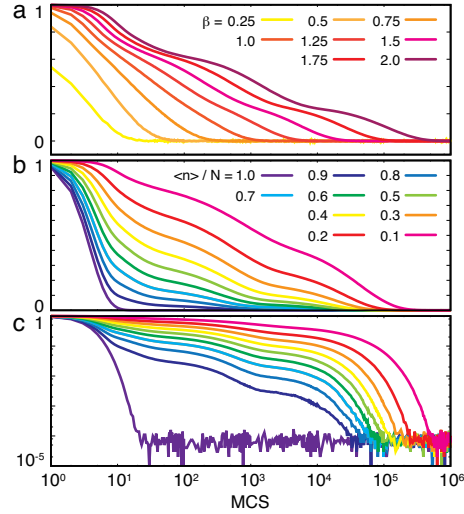


Figure S 2: Time evolutions of the average structural spin in the enzymatic MWC model against logarithmic time (Monte Carlo step). (a) Relaxation of the average number of structural spins to the equilibrium state at various temperatures. The equilibrium fraction of T-state molecules  $\mathcal{T}_{\text{eq}}$  depends on the temperature; therefore, the normalized ratio  $(\langle \mathcal{T} \rangle_{\text{ens}} - \mathcal{T}_{\text{eq}})/(1 - \mathcal{T}_{\text{eq}})$  was plotted.  $\langle n \rangle / N$  was set to 0.2. The different line colors show the time courses at different  $\beta$  values. (b) Relaxation of the average spin state to the equilibrium state at various values of  $\langle n \rangle$ . The equilibrium fraction of T-state molecules did not change with the changes in  $\langle n \rangle$ , and  $\langle \mathcal{T} \rangle_{\text{ens}}$  was plotted.  $\beta$  was set to 1.75. The different line colors indicate the time courses with different  $\langle n \rangle$  values. Each line is an ensemble average of 1000 samples. (c) Logarithm of  $\langle \mathcal{T} \rangle_{\text{ens}}$  plotted for (b).

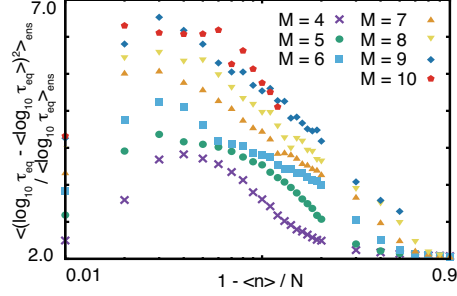


Figure S 3: The variance of logarithmic relaxation time for various values of  $M$ . The relaxation time of each sample was calculated in the same manner as in Fig. 4 in the main text. The variance was normalized by the averaged value. The horizontal axis denotes the difference of  $\langle n \rangle / N$  from 1.0 and the vertical axis denotes the variance of the logarithmic relaxation time. Each symbol indicates the variance for a different value of the number of modification sites  $M$ .

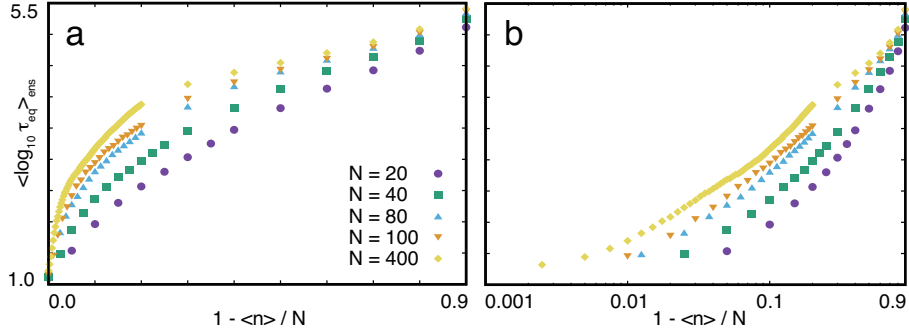


Figure S 4: The average of logarithmic relaxation time plotted against  $N$ . The relaxation time of each sample was calculated in the same manner as in Fig. 4 in the main text. The horizontal axis denotes the difference of  $\langle n \rangle / N$  from 1.0 (a) and its logarithmic plot (b). Different symbols indicate relaxation time for systems with different number of molecules  $N$ .

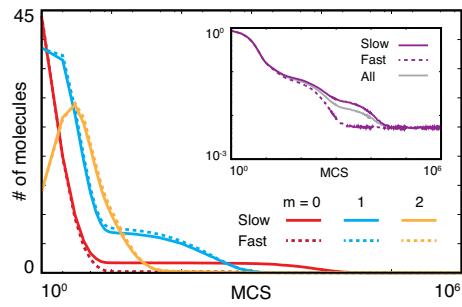


Figure S 5: Averaged dynamics for fast and slow groups in the bimodal distribution of the relaxation time with  $\langle n \rangle / N = 0.8$  and  $\beta = 1.75$ . The relaxation time of the samples in the fast group was faster than  $10^{3.3}$  MCSs, and that in the slow group was slower than  $10^{3.3}$  MCSs. The fast and slow groups had 416 and 584 samples, respectively. The red, blue, and yellow lines indicate the dynamics of molecules with zero, one, and two modified monomers, respectively. The dotted and solid lines indicate the dynamics of the fast and slow groups, respectively. Inset: Relaxation of the number of unmodified monomers  $\mathcal{U}$  of the fast and slow groups. Purple lines indicate the dynamics of each group, and the grey line indicates the dynamics of the whole sample.

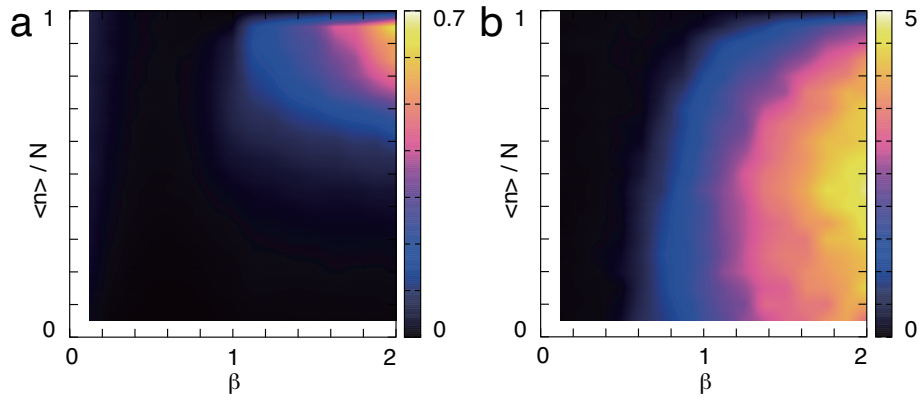


Figure S 6: Color maps of the variance of the logarithmic relaxation time and the number of unmodified monomers. (a)  $\langle [\log_{10} \tau_{\text{eq}} - \langle \log_{10} \tau_{\text{eq}} \rangle]^2 \rangle_{\text{ens}}$  against  $\beta$  and  $\langle n \rangle / N$ . The variance is indicated by the colors in the side bar. (b) Maximal variance in the number of unmodified monomers. This was calculated as the maximum variance among the ensemble in the time course after 20 MCSs. The logarithmic relaxation time was divided by the average  $\langle \mathcal{U} \rangle_{\text{ens}}$  and the result was subtracted from the analytically calculated value  $\langle (\mathcal{U} - \mathcal{U}_{\text{eq}})^2 \rangle_{\text{eq}} / \mathcal{U}_{\text{eq}}$ .

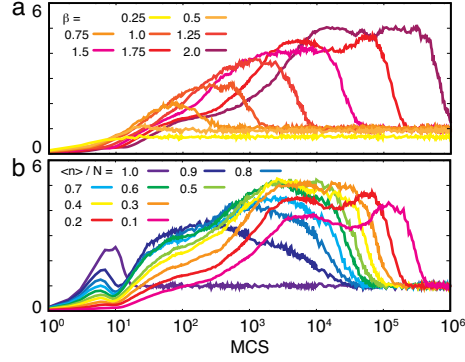


Figure S 7: Time evolution of the variance in the number of modification spins toward equilibrium in the enzymatic MWC model. (a) Relaxation of the variance in the number of modification spins to the equilibrium state at various temperatures. The variance was normalized by dividing it by the average.  $\langle n \rangle / N$  was set at 0.2. The different line colors indicate the time courses with different  $\beta$  values. (b) Relaxation of the variance in the state spin to the equilibrium state at various  $\langle n \rangle / N$  values.  $\beta$  was set as 1.75. The different line colors indicate the time courses with different  $\langle n \rangle / N$  values.

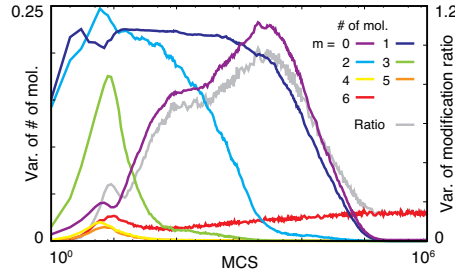


Figure S 8: Time evolution of the variance in the number of molecules with different modification spins at  $\langle n \rangle / N = 0.2$  and  $\beta = 1.75$ . The grey line indicates the variance in  $\mathcal{U}$ , and the other colored lines show the variance in the number of molecules normalized by division by  $N$ . The different colors indicate molecules with different numbers of modified monomers. Purple, blue, cyan, green, yellow, orange, and red indicate molecules with  $m = 0, 1, 2, 3, 4, 5, 6$ , respectively.